LABORATOIRE DE PHYSIQUE DE CLERMONT AUVERGNE

LHCB TEAM

MASTER 1 - SECOND SEMESTER INTERNSHIP

Study of the decay $B^+ \to K_1^+\gamma$ at LHCb.

Submitted by:

LECOMTE Samuel

Under the guidance of:

Régis LEFÈVRE

Internship from April, 8 2024 to June, 14 2024

Contents

Introduction

During the first year of my master's degree, I had the opportunity to do a 2-month internship in the LHCb team at the Clermont Physics Laboratory, supervised by Régis Lefèvre. My work was based on the study of the $B^+ \to K_1^+ \gamma$ decay. This is a rare mode which is of interest because it could be sensitive to physics beyond the Standard Model through the polarization of the radiative photon.

My internship is devoted to the first stages of this analysis, namely examining a dataset of simulated data, defining cuts to reduce the background and applying this selection to a set of reconstructed candidates in the LHCb data.

The first two chapters of this report contain the theoretical and technical elements relevant to this work. Subsequently, chapter 3 covers the reconstruction of the helicity angle and the definition of the preselection. Finally, chapter 4 presents preliminary results obtained applying the preselection to LHCb Run 1 data.

Keywords:

LHCb detector - Flavor physics - Radiative decays - Photon polarization

Chapter 1

Theoretical framework

1.1 The Standard Model

To date, the best theory to describe elementary particles and their interactions is the Standard Model (SM) of particle physics. Many key-points of this model have been tested experimentally, showing good agreement with predictions. However, some properties give ambiguous results, such as the anomalous magnetic moment of the muon [1], or are not even defined, such as the unification of general relativity with the Standard Model.

The Standard Model recognizes two families of elementary particles: fermions, which include quarks and leptons and have a half-integer spin, and bosons, which have an integer spin. Fermions are further subdivided into six quarks (up, down, strange, charm, beauty[1] and top), six leptons (electron, muon, tau, electron neutrino, muon neutrino and tau neutrino), and their 12 associated antiparticles. Quarks combine to form the basic building blocks of matter, in the form of mesons (composed of a quark and an antiquark) and baryons (composed of 3 quarks). Finally, bosons mediate the fundamental interactions: photons for the electromagnetic interaction, gluons for the strong interaction, and Z^0 and $W^\pm$ bosons for the weak interaction.

The decay being studied here process through the weak interaction.

1.1.1 Flavor changing mechanisms

In the Standard Model, the weak force is the only interaction inducing flavor changes. Furthermore, only flavor changing charged currents, by couplings to the $W^\pm$ bosons, are allowed. Flavor Changing Neutral Currents (FCNC), change of flavor without modification of the electric charge, are forbidden. The flavor of a quark, or even of a charged lepton, interacting with the Z neutral gauge boson, is conserved. Nevertheless, FCNC equivalent processes may occur at higher orders via loops of virtual particles.

An example of such a process is the $b \to s\gamma$ transition, depicted in Figure 1.1. In this case, a b quark undergoes a flavor change into a s quark, accompanied by the emission of a photon. This flavor change can only occur at higher orders via virtual particle loops involving a up-type quark and a $W^\pm$ boson. Because of its mass, the top quark dominates here. These radiative transitions are strongly suppressed in the SM, leading to very small branching ratios. They are thus of great interest in the search for signs of new physics, especially if it would allow FCNC.
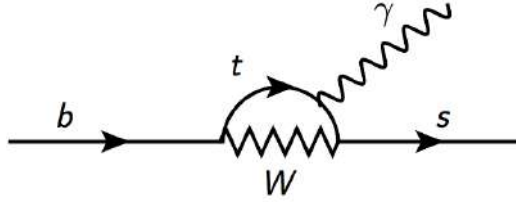
---

[1]Also called bottom quark.

Figure 1.1: Penguin diagram allowing the $b \to s\gamma$ transition in the SM.

1.1.2 CKM matrix

Flavor transitions can be described using the Cabibbo-Kobayashi-Maskawa (CKM) matrix. This is a unitary matrix that encodes the mixtures between the different flavors of quarks. Each element V_{ij} of this matrix represents the probability amplitude that a up-type quark i transforms into a down-type quark j. In the SM, the KM mechanism is the only source of CP violation for the quark sector.

1.2 Photon polarization and helicity

In particle physics, the polarization of a photon, which describes the orientation of its associated electromagnetic field, is closely linked to the notion of helicity, which is the projection of the photon's spin onto the direction of its motion. In the Standard Model, due to the $V-A$ structure of the weak interaction, photons emitted in $b \to s\gamma$ or $b \to d\gamma$ transitions are predominantly left-handed [2]. The presence of right-handed photons in these processes could be the signature of physics beyond the Standard Model [3].

Chapter 2

The LHCb experiment

2.1 The LHC

The Large Hadron Collider (LHC) [4], built beneath the Franco-Swiss border, is an instrument operated by CERN for particle physics research. It consists of a main ring, which has a circumference of 27 km, where two beams of protons circulating in opposite directions and colliding at a center-of-mass energy of up to 14 TeV. Prior to enter the main ring, these beams gain energy through a complex of smaller accelerators. A scheme of the acceleration chain is presented in Figure 2.1.
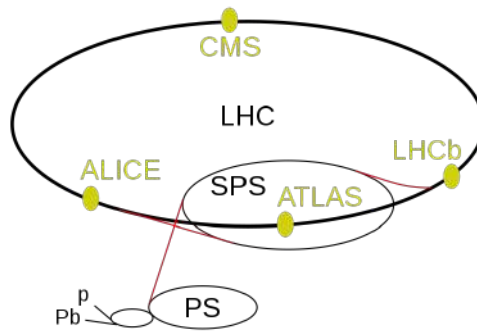

Figure 2.1: Layout of the CERN accelerator complex. The four interaction points are also depicted on the LHC ring.

Once introduced into the main ring, the proton beams, which are organized into bunches, collide at specific points, known as interaction points. It is at these locations that detectors are installed. The LHC is housing four main experiments: Alice, Atlas, CMS and LHCb. The first two are multi-purpose experiments studying for instance the Higgs boson and the top quark. They are also designed for direct searches of new physics. The Alice experiment is dedicated to heavy ions physics, in particular the study of the quark-gluon plasma. Finally, the LHCb detector [5] was designed to study flavor physics in particular CP violation and indirect searches for new physics through beauty hadrons rare decays. It is presented in more detail in the following.

2.2 The LHCb detector

The LHC presents a high production cross-section for $b\bar{b}$ pairs in forward and backward cones. To provide high-precision measurements, the detector is designed as a single-arm spectrometer,

oriented towards the forward cone. Figure 2.2 shows a side view of the detector, where all its components are represented.
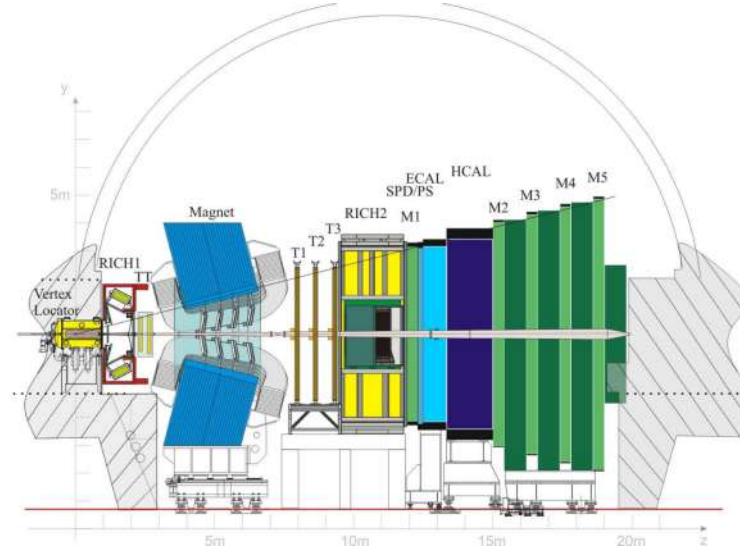

Figure 2.2: Side view of the LHCb detector.

2.2.1 Subsystems

To accurately reconstruct particles, identify them, and measure their properties, the detector is divided into several subsystems:

- **The VErtex LOcator (VELO)** is positioned around the interaction region and enables precise reconstruction of primary and secondary vertices.

- **The Tracker Turicensis (TT) and tracking stations (T1, T2, T3)** are responsible for reconstructing the trajectories of charged particles.

- **The dipole magnet** bends the trajectories of charged particles and is used to measure their momentum.

- **Two Cherenkov detectors (RICH1 and RICH2)** provide a speed measurement used to distinguish between different types of charged particles (specially pions, kaons and protons).

- **The calorimeters** determine the charged nature of incoming particles (SPD[1]), the differentiation between electrons/photons from other particles (PS[2]), and the measurement of their energy with the ECAL[3] and the HCAL[4].

- **The muon system** is used to identify muons, which are often present in the final states associated to B meson decays.

2.2.2 Track types

The combined information from the tracking sub-detectors allows for the reconstruction of particle trajectories from the interaction area to the calorimeters. Figure 2.3 shows the paths of different types of trajectories through the detector. In particular, the **Long tracks** are generally the best-defined and therefore the most used in physics studies.

---

[1]Scintillator Pad Detector   [3]Electromagnetic Calorimeter
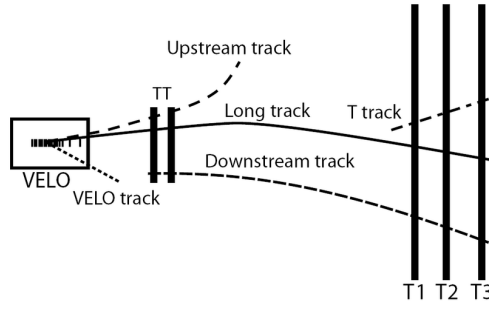[2]PreShower   [4]Hadronic Calorimeter

Figure 2.3: Track types at LHCb.

2.3 γ/π^0 reconstruction

Photons are reconstructed by combining information from the calorimeters. When a photon enters the calorimeters, it deposits energy. The profile of this energy deposition helps to determine whether the particle is a single photon or a decayed π^0. Those will leave two closely spaced or even overlapping deposits in the ECAL, corresponding to so-called resolved or merged π^0.

2.4 Charged PID

The identification of charged particles are mostly based on the analysis of the Cherenkov rings measured in the RICH detectors. The size of the ring produced is related to the particle's velocity. The momentum of the track being independently measured by the tracking system, this velocity measurement is, in turn, a measurement of the mass of the particle associated to the track. Indeed, if two particles have different masses and the same momentum, they do propagate at different speeds, resulting in the production of Cherenkov rings of different sizes.

2.5 LHCb trigger system

The trigger system employed by LHCb is designed to efficiently select events of interest from the large amount of data produced by the detector. The Level 0 (L0) trigger is hardware and reduces the event rate from 40 MHz to about 1 MHz [6] looking at high transverse energy deposits in the calorimeters and high transverse momentum (p_T) muons identified in the muon system. The higher-level triggers, HLT1 and HLT2, which operate entirely on software, refine this selection. The HLT1 makes a preliminary reconstruction of tracks and reduces the rate to about 70 kHz looking at a high p_T track with a large impact parameter with respect to the reconstructed proton-proton interaction points (primary vertices). The HLT2 further decreases the rate to few kHz, performing a full reconstruction of the events.

Chapter 3

Work on simulation samples

3.1 The $B^+ \to K_1^+ \gamma$ decay

The charged B^+ meson, with a mass of 5279.3 MeV/c^2 [7], is composed of an up quark and a bottom antiquark ($u\bar{b}$). This meson can decay into a $K_1^+\gamma$ state with a certain probability, known as the branching ratio. This branching ratio is unknown given the $B^+ \to K_1^+\gamma$ mode has never been observed. This is indeed one of the long term goal of the study initiated during my internship. The K_1^+ particle is not stable and decay via the strong force. In this study, we are considering the $K_1^+ \to K^+\omega$ decay mode, which has a branching ratio of about 11%. The ω itself also decays strongly: we are considering the dominant $\omega \to \pi^+\pi^-\pi^0$ mode, which corresponds to a branching ratio of 89.2%.

To reconstruct the $B^+ \to K_1^+\gamma$ decay, one has first to identify all the particle of the final state: the three tracks related to the K^+, π^+ and π^-, the energetic radiative photon as well as the two photon clusters associated to the π^0 decay. The intermediate resonances (ω and K_1^+) as well as the B^+ can then be reconstructed.

The objective of chapters 3 and 4 is to study this decay using both simulation and data samples. For what concerns the simulation study, the objective is threefold. Firstly, to understand how the data are organised. Secondly, to conduct an initial analysis of the signal, reconstructing the helicity angle. Thirdly, to design a preselection that will be applied to the data from the experiment in order to reject most of the background while keeping most of the signal.

3.2 Data organisation

All of my work was carried out on ROOT [8], a programming language derived from C++ published by CERN. The data, whether from simulation samples or real data samples, are contained in ROOT files called TFiles. These files are structured like trees. A TFile allows grouping different types of data (variables, histograms, etc.) in a single *large* folder. It typically contains a tree, which in turn ramifies into several branches. These branches serve to store the variables that contain the data. There are several methods of accessing the information contained in the branches. The simplest of these is to open the TFile in a terminal. This has the advantage of being quick, and I mainly used it to create graphs on the fly and to test preselection or fit parameters very easily. A second method that I have used frequently is C++ scripting. This has been used to set up more complex methods of data analysis and selection and to generate graphs with any desired layout.

3.3   About the background

As explained previously, to reconstruct the B decay of interest, one has to combine three tracks, a photon and a π^0. If no cut would be applied, any random combination of those would form a signal candidate. As an example, the π^0 itself, formed from two electromagnetic clusters, could be related to a real π^0 decay or be the association of two random electromagnetic clusters. Each of the final state objects could directly come from a proton-proton collision, from a strongly interacting resonance or from the decay of a long live particle.

In the Monte Carlo (MC), reconstructed objects can be matched to the true final state particles. Each B candidate can then be classified according to the matching of its decay products. The tool in charge of this classification is called *BackgroundCategory*. In our case, the candidates from the signal simulation samples really associated to the signal are classified as *quasi-signal* (BKGCAT = 10). *Quasi-signal* and not *signal* because in fact the decay was reconstructed as $B^+ \to K_2^+ \gamma$ with $K_2^+ \to \pi^0 K_1^+$ and $K_1^+ \to K^+ \pi^+ \pi^-$. The final state particles are the same as for the signal but the intermediate resonances are not.

Figure 3.1 shows the reconstructed mass for the B and ω mesons obtained on signal simulation samples. The distributions correspond ever to the candidates fully associated to the signal and to all the candidates (fully, partially or not associated to the signal decay products). One as to be careful, the apparent reduction in statistics is not a loss in signal efficiency but a reduction of the combinatorics, indeed one can have more than one candidate per event if the candidates are not required to be matched to the signal.

In the following, when designing the preselection, the candidates not fully matched to the signal will be used as a proxy of the background.
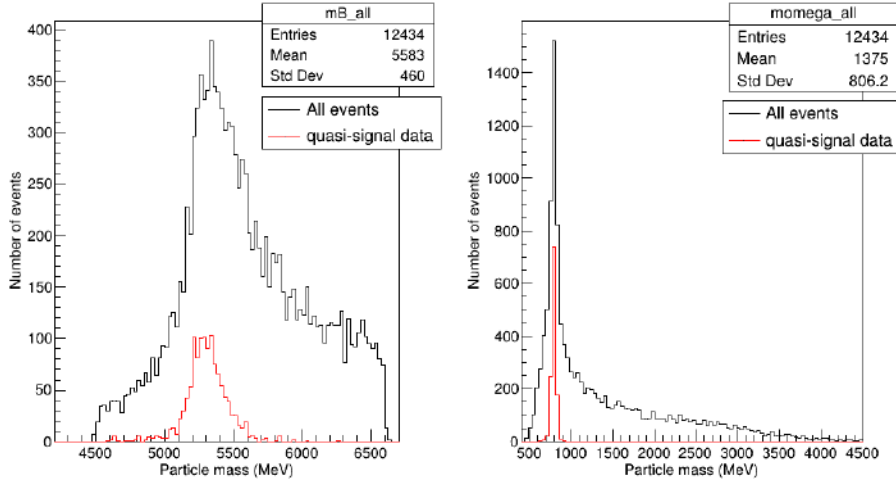

Figure 3.1: Reconstructed mass for the B (left) and ω (right) mesons from signal simulation samples. In black, the mass distributions for all the candidates; in red, the ones for the candidates fully associated to the signal.

3.4   Helicity angle

As introduced in section 1.2, it may be interesting to determine the helicity angle between the B^+ and K^+ mesons to be able to estimate the polarization of the radiative photon through a detailed study. I have only worked on the reconstruction of the helicity angle. First, I will

recompose the four-momenta of each particle from the p_x, p_y, p_z and E components. From this, I will be able to boost the B^+ and K^+ into the K_1^+ frame, and finally access the helicity angle.

For the simulation sample, as explain previously, reconstructed objects can be matched to the true final state particles. For candidates fully matched to the signal, all the true four-momentum are then accessible. This allows to check that all the calculations are correct but also to evaluate the expected resolution on the helicity angle.

The TTree contains individual components that are used to get four-momenta objects using the TLorentzVector class from ROOT. As explained previously, the ω intermediate resonance is not present in the TTree and has to be reconstructed from its decay products.

3.4.1   Boosting to the K_1^+ frame

Once all the four-momenta have been obtained, we boost them to the K_1^+ frame. In this frame, we expect the ω and K^+ momenta to be back-to-back, while the γ and B momenta should be in the same direction. Indeed, in any frame, the four-momentum conservation implies

$$\vec{p}_{B^+} = \vec{p}_{K_1^+} + \vec{p}_\gamma \ .$$

So in the K_1^+ frame,

$$\vec{p}_{B^+} = \vec{p}_\gamma \ .$$

Similarly, one has in any frame,

$$\vec{p}_{K_1^+} = \vec{p}_{K^+} + \vec{p}_\omega \ .$$

So in the K_1^+ frame,

$$\vec{p}_{K^+} = -\vec{p}_\omega \ .$$

This has been checked, looking at the cosines of the angles between the momentum vectors obtained in the K_1^+ frame.

3.4.2   Acceptance and resolution

The cosine of the helicity angle can then be obtained as:

$$\frac{\vec{p}_{B^+} \cdot \vec{p}_{K^+}}{\|\vec{p}_{B^+}\| \times \|\vec{p}_{K^+}\|} \ ,$$

where the momenta are evaluated in the K_1^+. Figure 3.2 shows the obtained helicity distribution. According to the physical parameters introduced in the simulation, the generated helicity distribution is flat in cosine. The effect we obtain here is due to the acceptance of the detector which seems to introduce a distortion relatively easy to control. Figure 3.3 shows that the helicity angle is very well reconstructed: the associated resolution will have a negligible impact on the measured distribution.

3.5   Preselection

To build the preselection, one first need to identify the variables that can be used. To do so, I have grouped them in five categories.
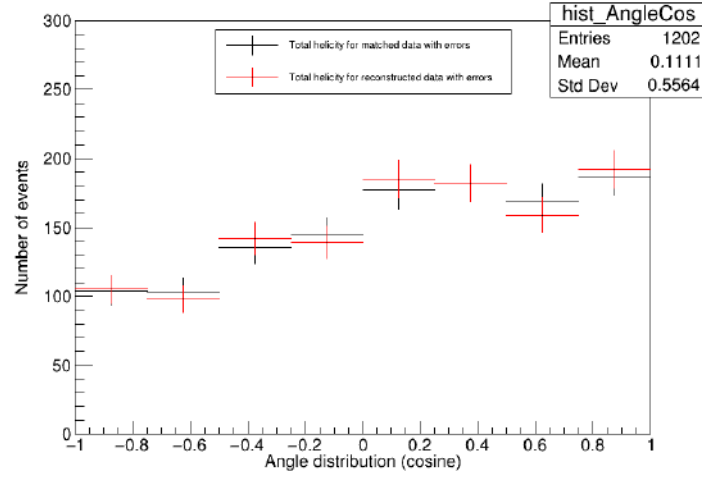
Figure 3.2: Cosine of the helicity angle from the true (black) and reconstructed (red) kinematics.
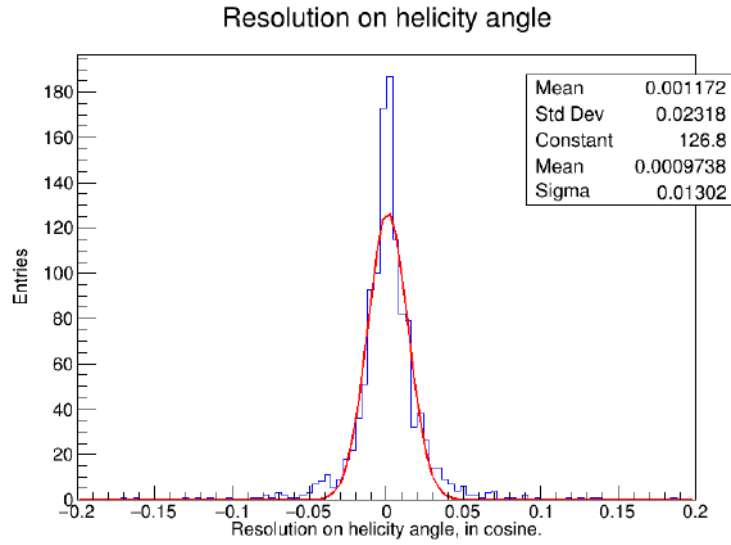

Figure 3.3: Distribution of the difference between the true and reconstructed cosines of the helicity angle.

Tracks (π^+, π^-, K^+)

The information about the particle identification (PID) of charged particles, as pions, kaons or protons, are collected in so-called ProbNN variables: ProbNNpi, ProbNNk and ProbNNp. Those are neural network outputs bounded between 0 and 1. Figure 3.4 shows as an example the ProbNNk distribution for the track associated to the reconstructed π^+. The higher the value of ProbNNk, the more likely the track is associated to a kaon. Here and in following plots, as already mentioned, the signal corresponds to fully matched signal candidates while not fully matched candidates from the MC signal samples are used as a proxy of the background.

For tracks, we also used the transverse momentum and a variable called IPCHI2_OWNPV. The later indicates whether the track may in fact comes directly from a primary vertex (proton-proton interaction point). The higher the value of the variable, the less likely it is.
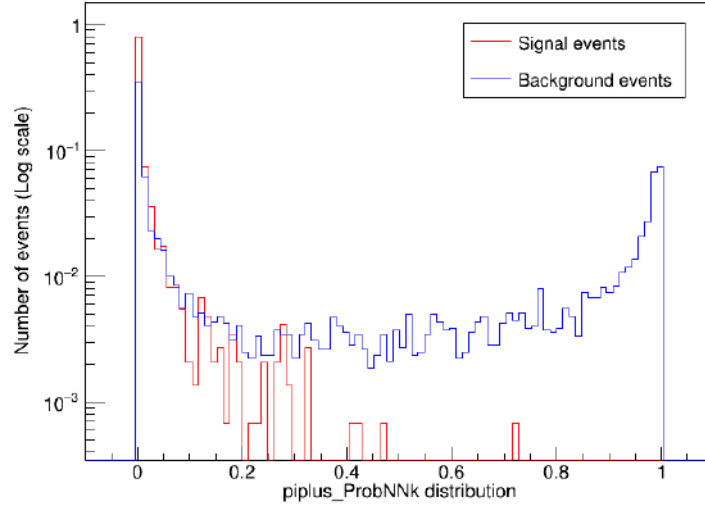
Figure 3.4: ProbNNk distribution for the track associated to the reconstructed π^+ for signal (red) and background (blue).

Neutral particles(π^0, γ, γ_0, γ_1)

For neutral particles of the final state, the PID information is contained in several variables:

- gammaCL: indicates whether or not the particle under consideration is likely to be associated with an electromagnetic shower.

- isPhoton: differentiates photons from merged π^0.

- isNotE: denotes whether the particle in question could in fact be associated to an electron.

To this we add the transverse momentum. Figure 3.5 shows the gammaCL distribution for the radiative photon candidate. The spike around 0 corresponds to noise.
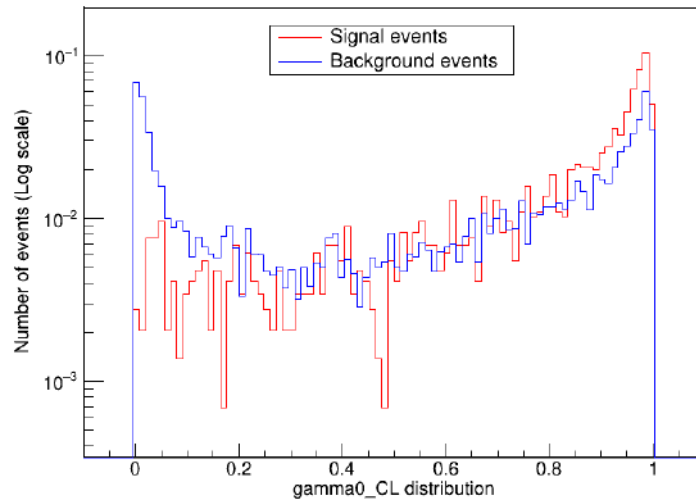

Figure 3.5: GammaCL distribution for the radiative photon candidate for signal (red) and background (blue).

B^+ meson

For the B^+ meson, in addition to the transverse momentum as previously, we are mainly looking at topological variables:

- FD_OWNPV: represents the distance between the primary vertex and the decay vertex of a particle, measured in mm.

- FDCHI2_OWNPV: the scare of the significance of the separation between the primary vertex and the decay vertex of a particle.

- ENDVERTEX_CHI2: reflects the quality of the decay vertex. A high value may indicate that the tracks used to form the vertex are in fact not compatible with coming from the same vertex.

- DIRA_OWNPV: calculated from the cosine of the angle between the particle's momentum vector and the line linking the primary vertex to the particle's decay vertex. It is expected to be close to 1 given the particle is supposed to move from its production point to its decay vertex.

The distributions of the variables associated to the B^+ have a much more tenuous separation between signal and background. This is because cuts on some of these variables have already been applied when building the input TTree we are using. Else, the combinatorial background and so the number of candidates per events would have increase exponentially. As shown on figure 3.6, it is better not to cut on these variables at the preselection level.
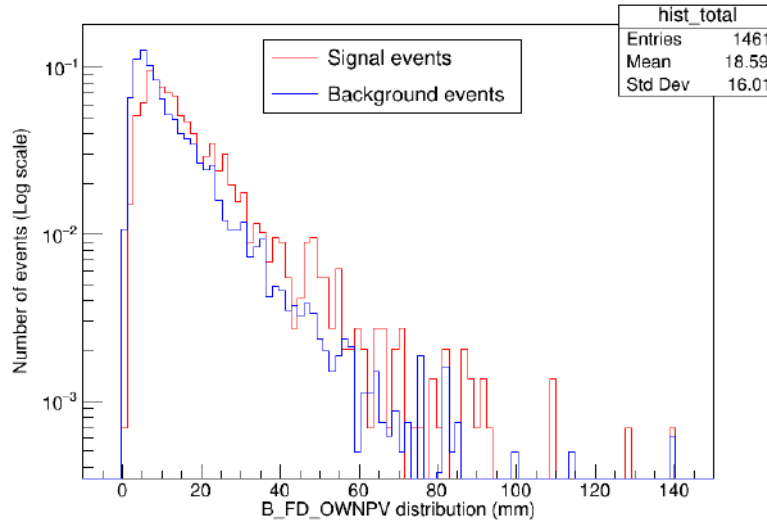

Figure 3.6: FD_OWNPV distribution for the B^+ candidate for signal (blue) and background (red).

Invariant masses

For the ω and the K_1^+ intermediate resonances, the reconstructed invariant masses are considered. In the TFiles, this corresponds to the following variables: B_M1234 for the ω and B_M01234 for the K_1^+ (each number represents a final state particle[1]). Figure 3.7 show the

---

[1] $0=K^+$, $1=\pi^+$, $2=\pi^-$, $3=\gamma$, $4=\gamma_0$, $5=\gamma_1$ (radiative)

corresponding distributions: a significant part of the background can be rejected with cuts wide enough to preserve all the signal.
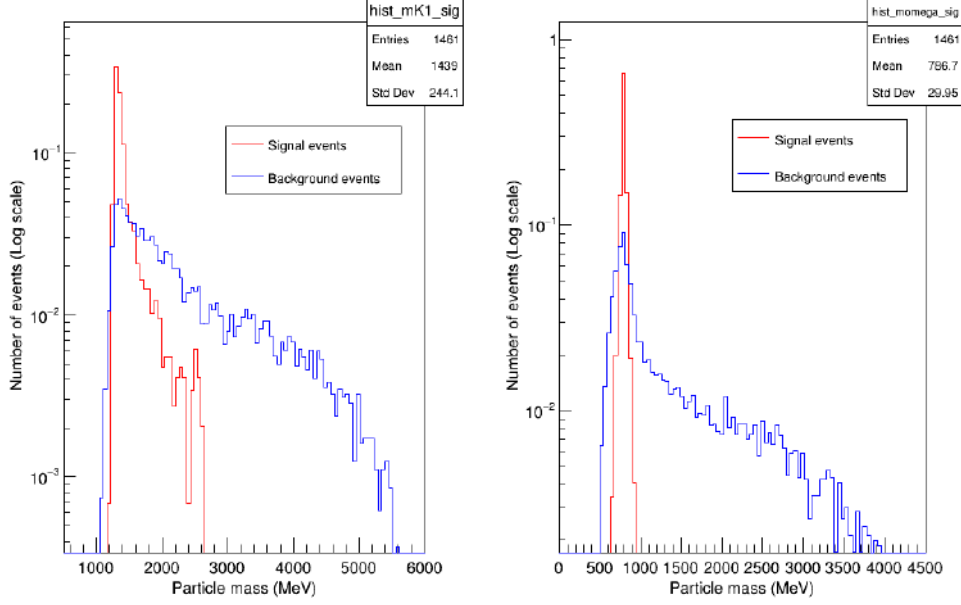

Figure 3.7: Reconstructed invariant masses for the K_1^+ (left) and ω (right) candidates, for signal (red) and background (blue).

3.6 Preselection cuts

Appendix 4.3 shows the full set of variables that have been studied. The following cuts have been chosen in order to reduce the background without affecting much the signal:

For $\pi^\pm$:
$$\begin{cases} \text{ProbNNpi} > 0.2 \\ \text{ProbNNk} < 0.8 \\ \text{ProbNNp} < 0.8 \end{cases}$$

For photons:
$$\begin{cases} \text{gammaCL} > 0.2 \\ \text{isPhoton} > 0.5 \end{cases}$$

For K^+:
$$\begin{cases} \text{ProbNNpi} < 0.8 \\ \text{ProbNNk} > 0.2 \\ \text{ProbNNp} < 0.8 \end{cases}$$

For invariant masses:
$$\begin{cases} \omega \text{ mass } < 1500 \text{ MeV} \\ K_1^+ \text{ mass } < 3000 \text{ MeV} \\ 4500 \text{ MeV} < B^+ \text{ mass } < 7000 \text{ MeV} \end{cases}$$

The invariant mass cuts are very loose at this level to allow the identification of specific backgrounds, if any. For the B^+ mass, no tight cut can be used in any case given the signal yield will have to be estimated fitting, with signal and background components, the B^+ invariant mass distribution.

In addition, the trigger has to be taken into account. For the trigger to be reliable, specific trigger lines are used at each of the three trigger levels. This comes with an unavoidable loss in signal efficiency but also with a large background reduction.

To be able to factorize the efficiencies, the cuts are applied in sequence and the efficiency of a

13

given cut is defined as the following ratio:

$$\epsilon(\text{cut i}) = \frac{\text{Number of events passing the previous cuts and cut i}}{\text{Number of events passing the previous cuts}}$$

To simplify the reading, efficiencies are evaluated by groups of cuts:

- Charged PID: ProbNNpi, ProbNNk and ProbNNp cuts applied to the π^+, π^- and K^+ candidates;
- Neutral PID: gammaCL and isPhoton cuts applied to the radiative photon and the two photons from the π^0;
- Invariant mass: invariant mass cuts applied to the reconstructed ω, K_1^+ and B^+;
- Triggers: trigger cuts applied at L0, HLT1 and HLT2.

The signal efficiencies are reported in the following table.

Cut	Efficiency
Charged PID	91%
Neutral PID	81%
Invariant Mass	100%
Triggers	76%
Total Efficiency	57%

Table 3.1: Preselection signal efficiencies.

Given there are three tracks to identify, the charged PID efficiency corresponds to an efficiency per track of about 97%. For neutral PID cuts, the dominant factor comes from the isPhoton cut on the radiative photon. However, specific backgrounds with high energy π^0 are often the more problematic for radiative studies, this is the only way to reduce them. The trigger efficiency on signal events passing the preselection is found to be relatively good.

The total preselection signal efficiency is 57%. This will have to be compared to the background reduction it allows on data. This is the object of the next chapter.

Chapter 4

Looking at Run 1 data

4.1 Data used

The analysis is now based on data samples collected during Run 1. Those are inclusive samples obtained combining an energetic photon with three tracks and a π^0, without any assumption on potential intermediate resonances. Hence, the combinatorial background is very important and those samples are huge. To pre-filter them, the invariant mass cuts defined in the previous section are used. We observed that this allows to reduce the amount of data by a factor of about 30.

4.2 Data filtering

4.2.1 Search for specific backgrounds

To identify specific backgrounds, we looked at the various invariant mass distributions one can obtain combining two, three or four out of the five particles in the final state. The most relevant distributions are reported in figure 4.1. Looking at the $K^+\pi^-$ invariant mass, two clear peaks associated to the $K_0^*(892)$ and to the D^0 mesons can be identified. Another specific background can be associated to $D^0 \rightarrow K^-\pi^+\pi^0$ decays. For what concerns the $\pi^+\pi^-\pi^0$ invariant mass distribution, a possible η contribution appears on the zoom at low mass.

The last point is not a problem given the η region does not overlap with the ω one. On the other hand, the $K_0^*(892)$ and D^0 resonances have to be vetoed. The following cuts are then applied:

- $m_{K^+\pi^-} \notin [840 - 970]$ MeV and $\notin [1750 - 1970]$ MeV

- $m_{K^+\pi^-\pi^0} \notin [1750 - 1970]$ MeV

For the signal MC, these vetoes introduce an additional efficiency of 85%. The data sample is reduced by about a factor 1.6.

4.2.2 Applying the preselection

Applying the preselection defined in the previous chapter, the data sample is further reduced by a factor close to 6. To be more precise, the fraction of candidates passing the trigger and PID cuts of the preselection is 16%, to be compared to 57% one has for the signal.
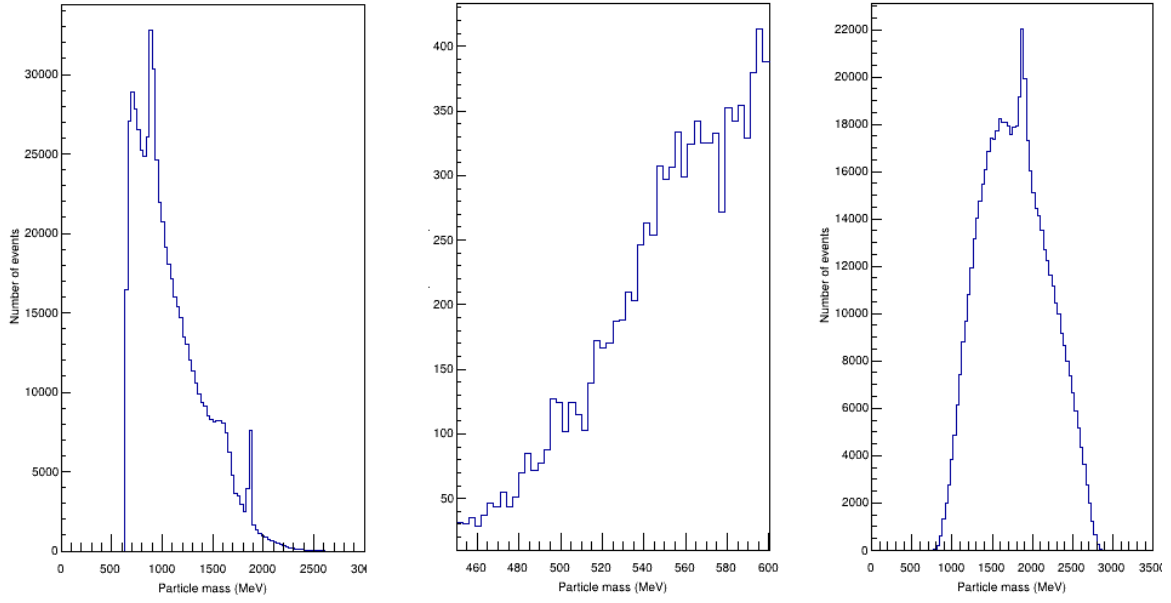
Figure 4.1: $K^+\pi^-$ (left), $\pi^+\pi^-\pi^0$ (middle) and $K^+\pi^-\pi^+$ (right) invariant mass distributions obtained on Run 1 pre-filtered data. For the middle plot, this is in fact a zoom at low mass.
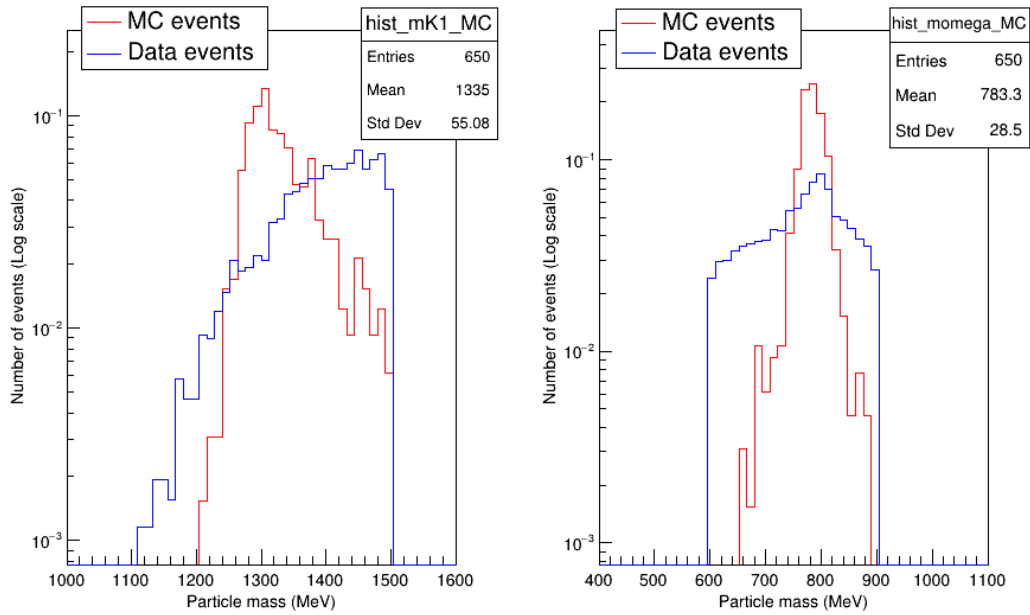

Figure 4.2: Invariant mass distributions obtained for the K_1^+ (left) and the ω (right). The histograms are normalized to unity area. The red histograms corresponds to MC signal candidates, the blue one to the Run 1 data.

16

Globally, the reduction factor obtained on the data inclusive samples is around 300. Yet, still about 100,000 candidates passes the overall preselection, just for Run 1. To focus on the decay channel of interest, we then apply more stringent cuts on the intermediate resonances:

$$\begin{cases} 600 < \omega \text{ mass (MeV)} < 900 \\ K_1^+ \text{ mass (MeV)} < 1500 \end{cases}$$

On signal MC, the efficiency of these cuts is 78%. The 22% loss corresponds to the K_1^+ tail at high mass. Only about 2,600 data events passes those tighter mass cuts.

The invariant mass distributions obtained for the ω and the K_1^+ are compared to the signal MC one on figure 4.2. For the ω, a clear peak is visible on the data. This is not the case for the K_1^+.

4.3   Not a serious attempt

An attempt to fit the B^+ mass distribution obtained on the remaining Run 1 candidates is shown in figure 4.3. The probability density function used is the sum of:

- for the signal, a gaussian distribution with μ and σ fixed to the values obtained fitting the MC signal events (respectively 5294 ± 5 MeV and 106 ± 4 MeV);

- for the background, the sum of an exponential function and of a flat distribution.

The exponential function used to accommodate the background at low mass is completely add-hoc. Correlatively, as shown on the figure, the fit probability is not good. Further studies would be required to evaluate the shape associated to partially reconstructed backgrounds. Usually, distribution based on the ARGUS function [9] and validated on dedicated MC samples are used. Even if the bump would be confirmed, given that there is no sign of K_1^+ in the $K^+\omega$ invariant mass distribution, it may not be associated to the decay mode we are searching for. Yet, this is encouraging.
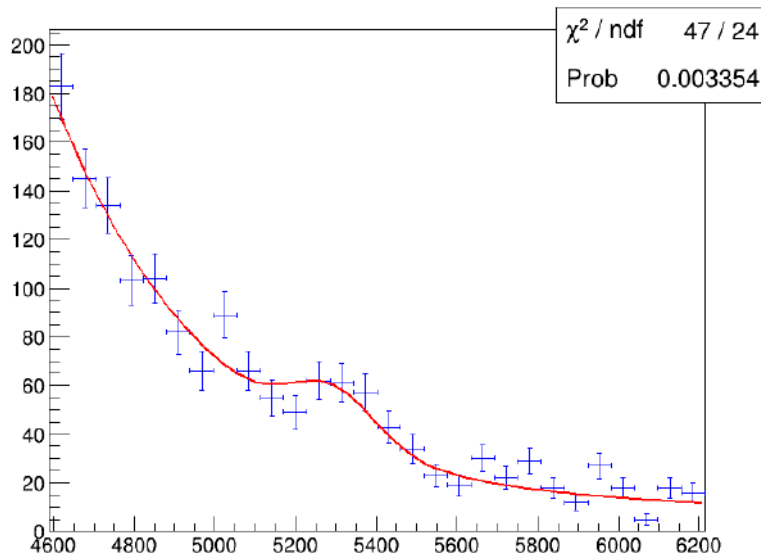

Figure 4.3: An attempt to fit the data.

Conclusion

My work during this internship focused on the study of the $B^+ \to K_1^+(K^+\omega)\gamma$ radiative decay. I studied the effects of the detector on the reconstructed helicity angle, both in terms of acceptance and resolution. In addition, I also developed a preselection that could be use to identify this channel in the LHCb dataset, on simulation samples but also on data samples to identify the specific backgrounds to be vetoed.
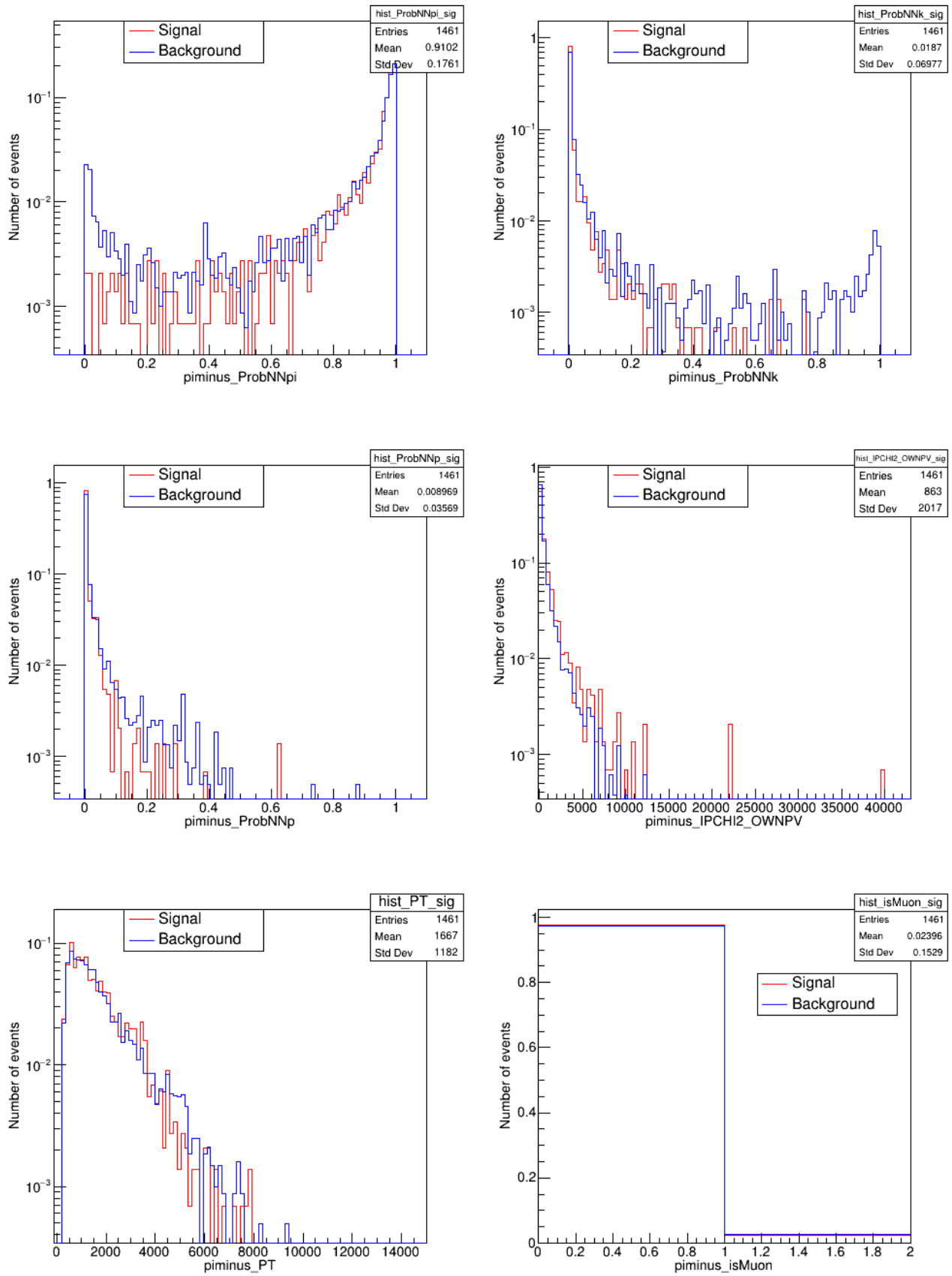
The short-term prospects are the integration of Run 2 data together with the implementation of a multivariate analysis to further reduce the background. It may very well be that Run 1 and Run 2 data will not be sufficient to really measure this decay. In that case, the data being collected in Run 3 are expected to significantly increase the statistics, a factor of three to four being expected.
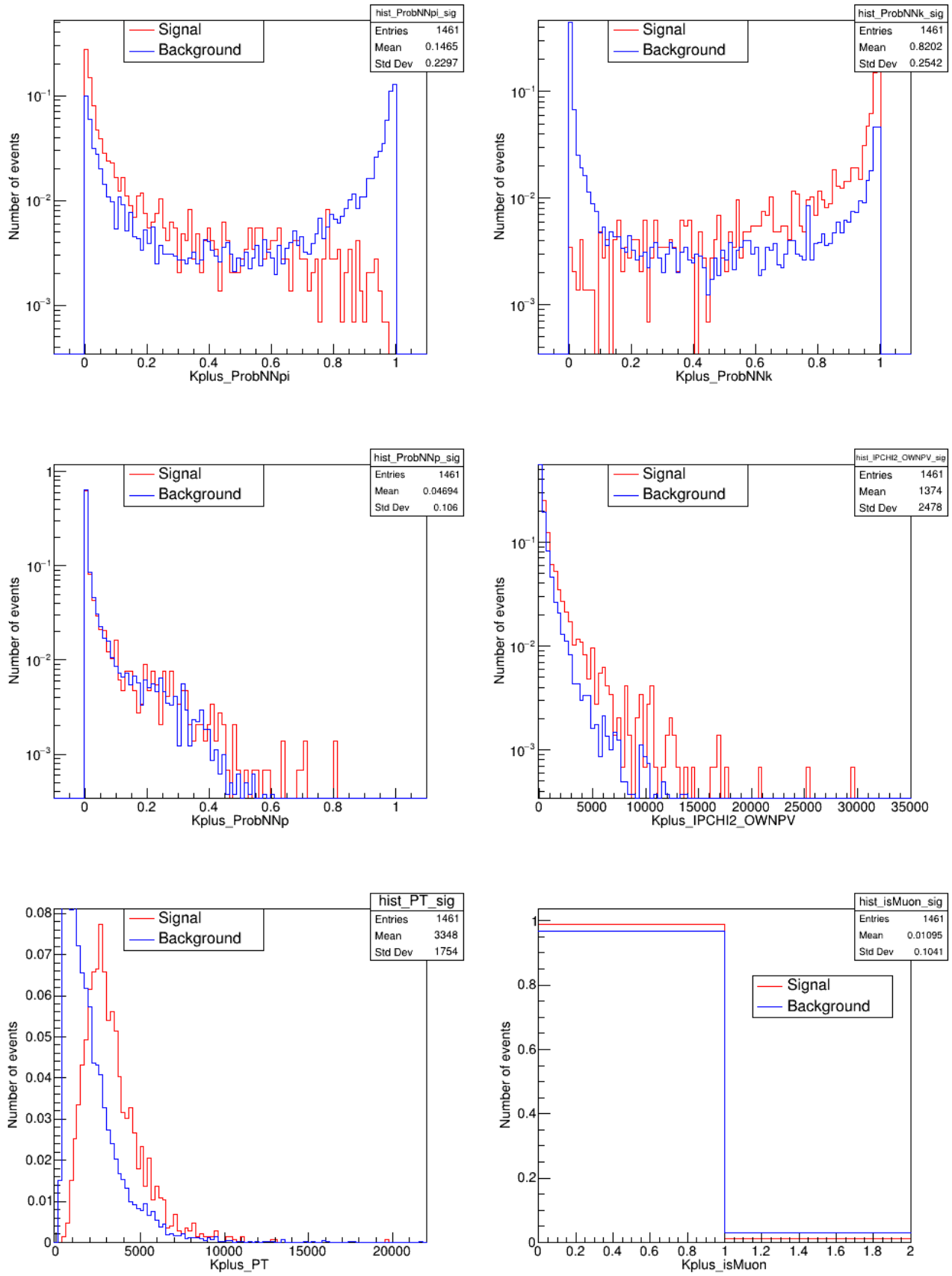
Bibliography

[1] T. Marc, *Muon g-2 doubles down with latest measurement, explores uncharted territory in search of new physics*, 2023. [Online]. Available: https://news.fnal.gov/2023/08/muon-g-2-doubles-down-with-latest-measurement/.

[2] L. Collaboration. "In pursuit of right-handed photons." (2020), [Online]. Available: https://cerncourier.com/a/in-pursuit-of-right-handed-photons/.

[3] F.-S. Yu, E. Kou, and C.-D. Lü, "Photon polarization in the b $\rightarrow$ sγ processes in the left-right symmetric model," *Journal of High Energy Physics*, vol. 2013, 2013, ISSN: 1029-8479. DOI: 10.1007/jhep12(2013)102. [Online]. Available: http://dx.doi.org/10.1007/JHEP12(2013)102.

[4] O. S. Brüning, P. Collier, Lebrun, *et al.*, *LHC Design Report* (CERN Yellow Reports: Monographs). Geneva: CERN, 2004. DOI: 10.5170/CERN-2004-003-V-1. [Online]. Available: https://cds.cern.ch/record/782076.

[5] R. Antunes-Nobrega, A. França-Barbosa, Bediaga, *et al.*, *LHCb reoptimized detector design and performance: Technical Design Report* (Technical design report. LHCb). Geneva: CERN, 2003. [Online]. Available: https://cds.cern.ch/record/630827.

[6] R. Aaij *et al.*, "Lhcb trigger and its performance," *Journal of Instrumentation*, vol. 9, no. 09, 2014. DOI: 10.1088/1748-0221/9/09/C09015. [Online]. Available: https://iopscience.iop.org/article/10.1088/1748-0221/9/09/C09015.

[7] R. Workman *et al.*, *Particle Data Group*. 2022. [Online]. Available: https://pdg.lbl.gov/2022/tables/rpp2022-tab-mesons-bottom.pdf.

[8] R. Brun and F. Rademakers, *Root - an object oriented data analysis framework*, Proceedings AIHENP'96 Workshop, Lausanne, Sep. 1996, Nucl. Inst. & Meth. in Phys. Res. A 389, https://root.cern, 1997.

[9] H. Albrecht, R. Gläser, G. Harder, *et al.*, "Search for hadronic b→u decays," *Physics Letters B*, vol. 241, no. 2, pp. 278–282, 1990, ISSN: 0370-2693. DOI: https://doi.org/10.1016/0370-2693(90)91293-K. [Online]. Available: https://www.sciencedirect.com/science/article/pii/037026939091293K.
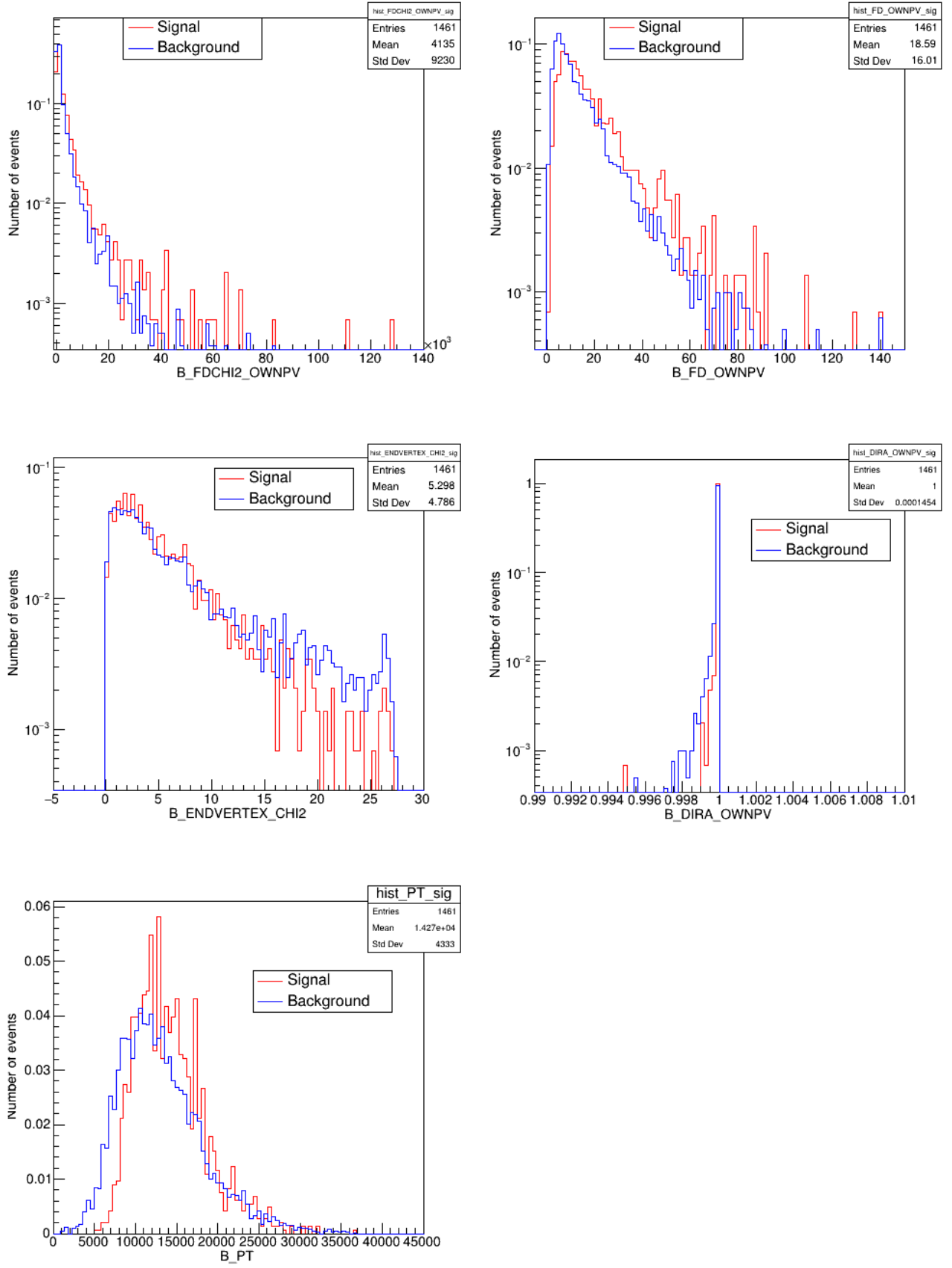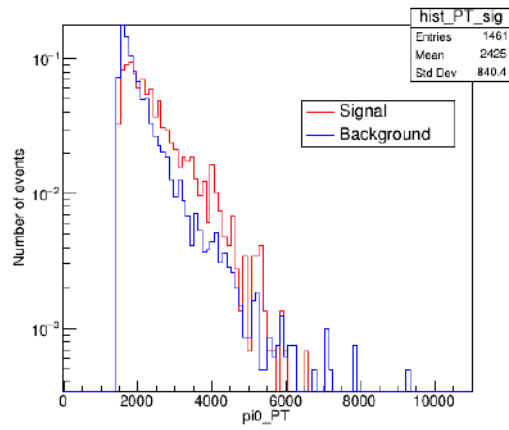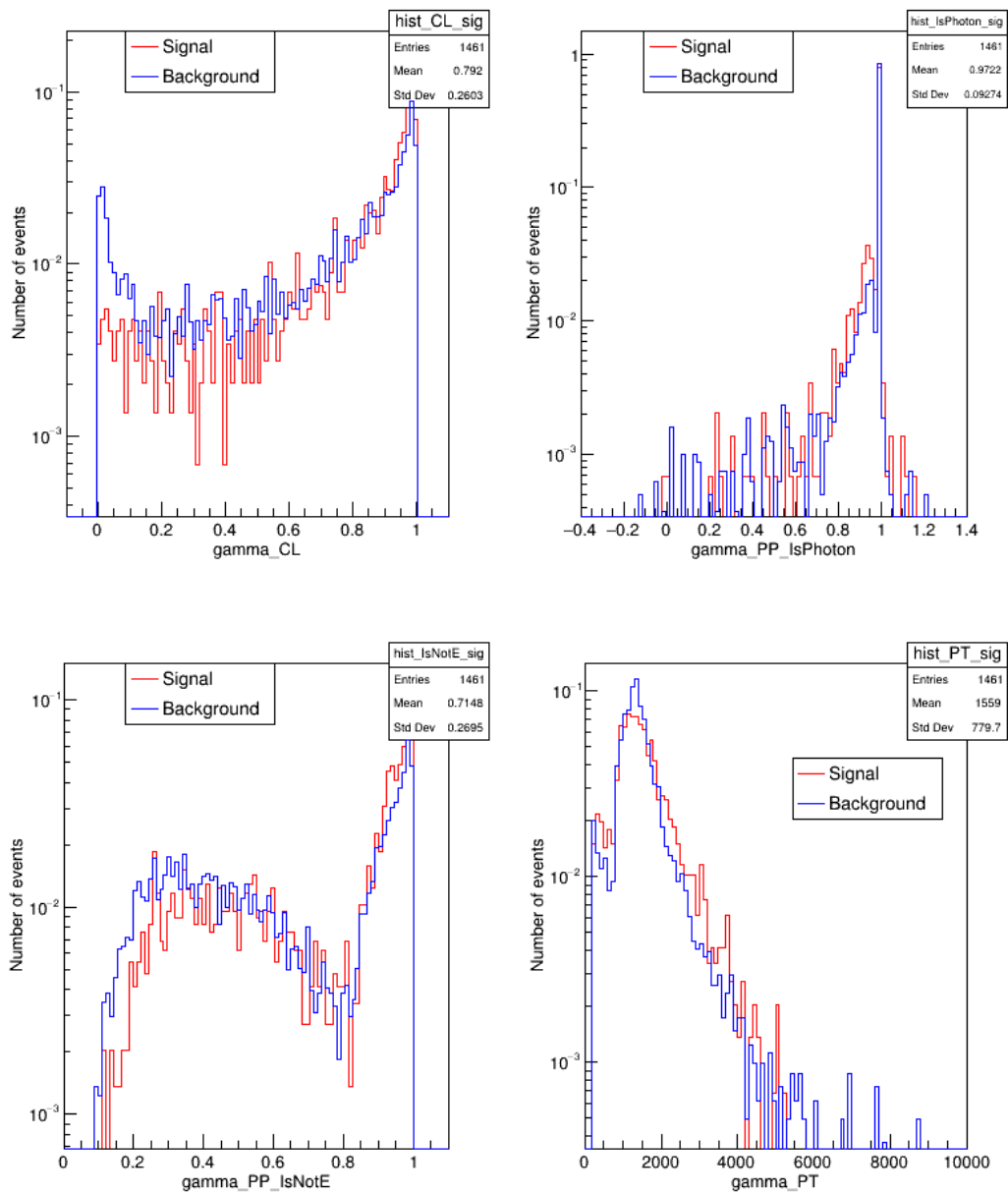
Appendices

Presentation of all the variables analyzed to design the preselection.

Figure 4: π^- variables.

B

Figure 5: π^+ variables.

C

Figure 6: K^+ variables.

D

Figure 7: B^+ variables.

E

Figure 8: π^0 variable.

Figure 9: Variables associated to the first electromagnetic cluster of a π^0.
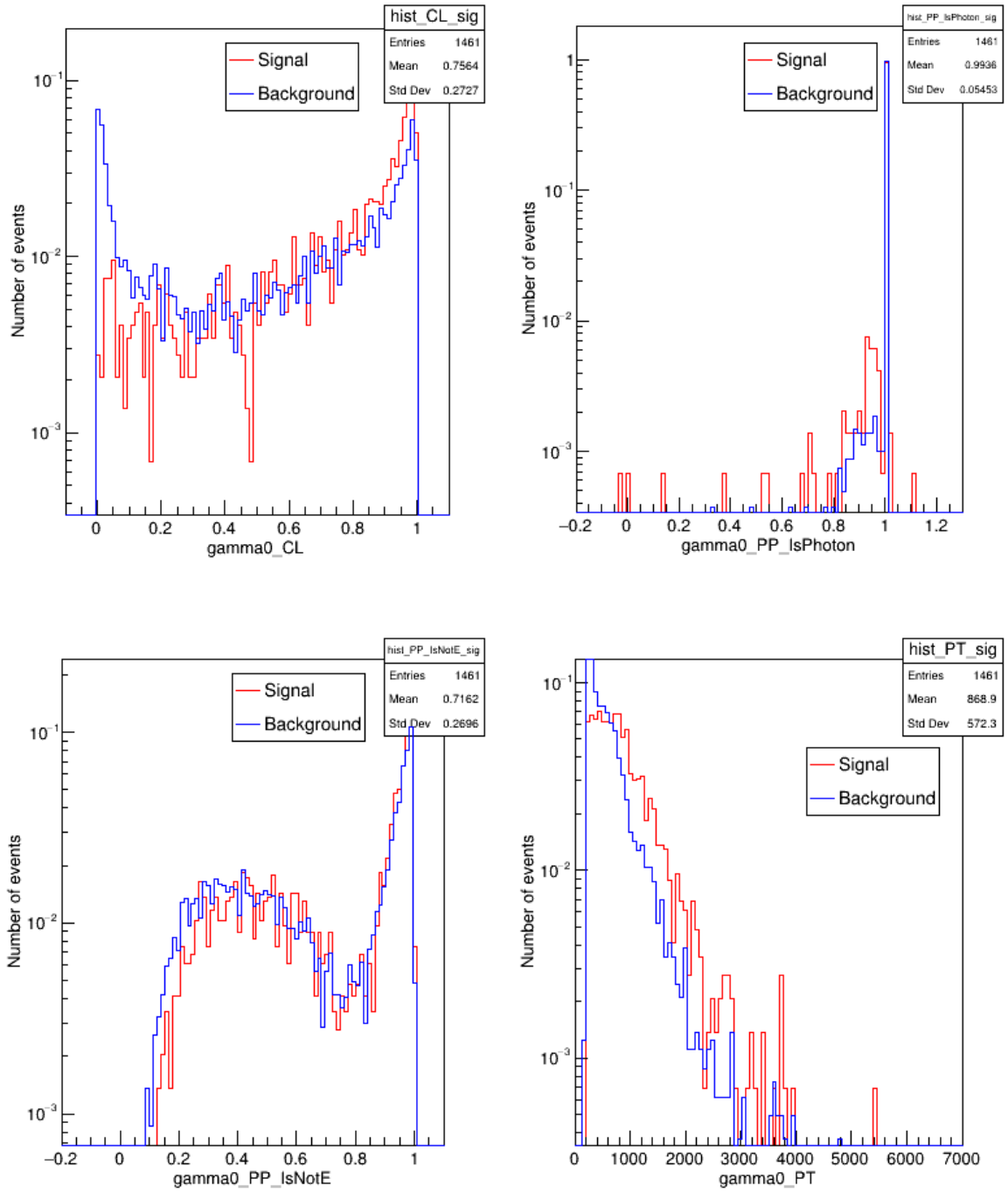
F

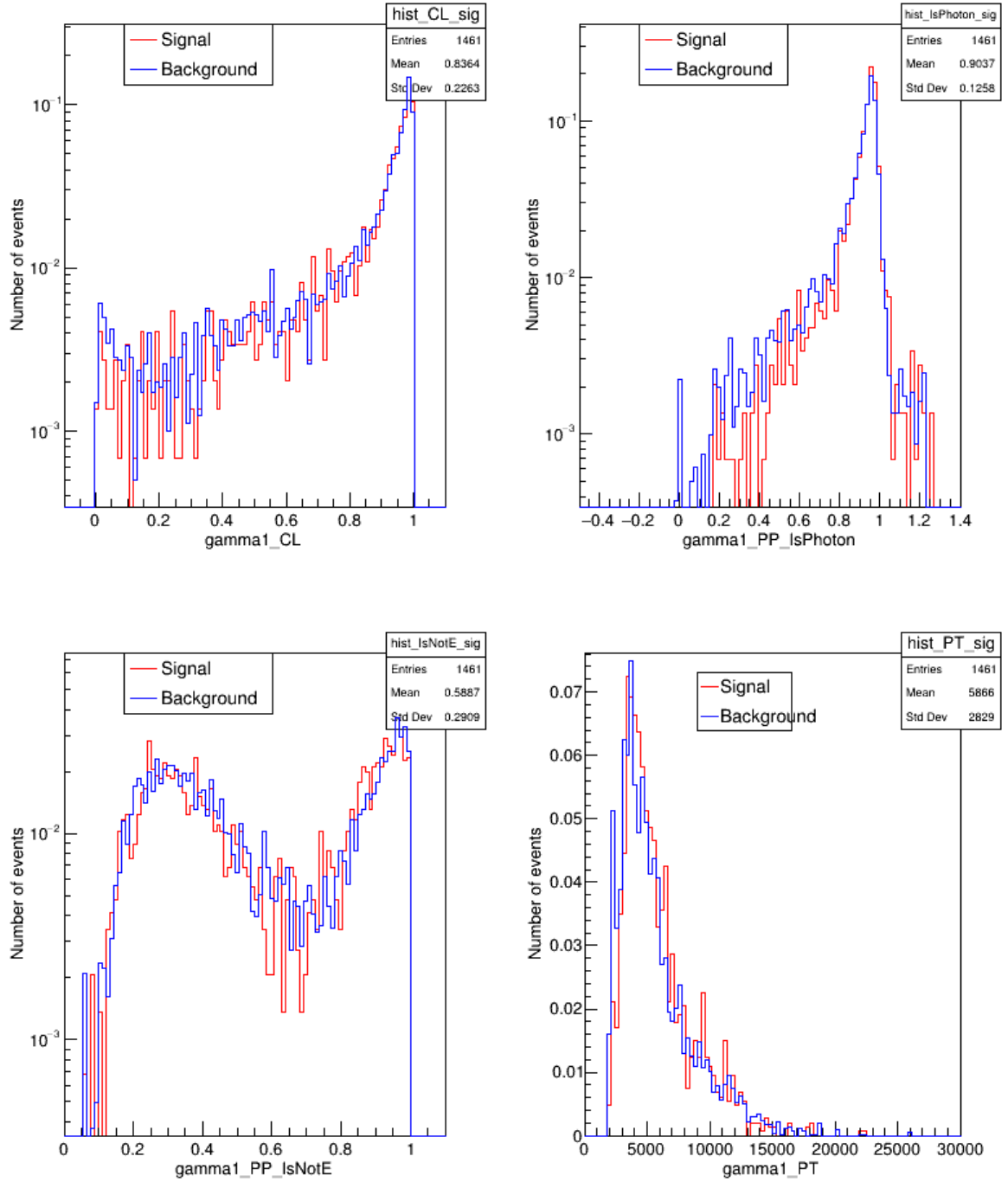Figure 10: Variables associated to the second electromagnetic cluster of a π^0.

Figure 11: Variables associated to the radiative photon.

H